Research Article Vol. 34, No. 8 / 20 Apr 2026 / Optics Express 13803
Optics EXPRESS

Trajectory control of a gimbaled prism for hemispherical pointing in CubeSat optical communications

RENÉ RÜDDENKLAU,[1,2,*] LUKAS RUPERT RODECK,[1] AND HANNES ZEIHSEL[1]

[1]Optical Satellite Links, Institute of Communications and Navigation, German Aerospace Center (DLR), Münchenerstr. 20, 82234 Weßling, Germany
[2]Mechatronics and Power Electronics Institute (MPEI), Technische Universität Wien, Gußhausstr. 27–29, Vienna, Austria
*rene.rueddenklau@dlr.de

Abstract: Free-space optical communications on CubeSats require precise pointing mechanisms to maintain stable links. State-of-the-art CubeSat-sized laser communication terminals rely on satellite body pointing, which imposes constraints on system flexibility. This paper presents the proposed control strategy of a gimbaled-prism-based coarse pointing assembly for hemispherical pointing in CubeSat optical communications. The gimbal design employs a compact mechanical structure with direct-drive actuation for azimuth and elevation control. A hierarchical control strategy is implemented, combining a cascaded servo control loop with an s-curve profiler for ephemeris-based pointing and a second-order trajectory controller for fine pointing assembly offloading. Therefore, the dynamics of the low-level controller can be decoupled from the trajectory control design. The performed experimental validation includes hardware characterization, system response identification, and closed-loop performance analysis, demonstrating the capability to achieve accurate and stable pointing of the developed coarse pointing assembly. Results confirm that the proposed approach meets stringent dynamics and stability requirements while maintaining a pointing accuracy suitable for CubeSat optical communication applications.

Published by Optica Publishing Group under the terms of the Creative Commons Attribution 4.0 License. Further distribution of this work must maintain attribution to the author(s) and the published article's title, journal citation, and DOI.

1. Introduction

Free-space optical communications on CubeSats are becoming a mature technology, as shown by the increasing number of missions and successful demonstrations [1–6]. As a consequence, each demonstrated laser communication terminal (LCT) is potentially eligible to be offered as a commercial product [7]. However, all of these LCTs require that the body pointing of the satellite is within a defined specification in terms of pointing accuracy and pointing drift rate. Therefore, the next reasonable step is to achieve pointing that is as independent as possible from the satellite's orientation in order to further optimize pointing for a different payload or for power generation via the solar panels during data transmission. The actuators used are often referred to as coarse pointing assembly (CPA) and are usually used in combination with a fine pointing assembly (FPA). This allows the FPA to compensate for high-frequency pointing jitter, while the CPA extends the field of regard (FOR). It simultaneously ensures that the FPA is offloaded, such that it can reserve as much of its limited deflection range as possible. Successful space missions with a CubeSat-compatible system of this type have not yet been published. However, there are efforts to build such a system and demonstrate it in orbit.

Facebook defined basic design requirements for such a system in 2017, showing a periscope configuration [8]. The hemispherical or near-hemispherical FOR was pointed out as an important

#580830 https://doi.org/10.1364/OE.580830
Journal © 2026 Received 1 Oct 2025; revised 12 Feb 2026; accepted 30 Mar 2026; published 7 Apr 2026

Optics EXPRESS

aspect. Other relevant features are open-loop pointing accuracy, peak slew rate, and size, weight, and power (SWaP) requirements. A similar design is also targeted for the ease of launch lock integration [9]. Space environment compatibility is important to consider, but the constraints in size do not allow certain CPA configurations that would be suitable for larger spacecraft [10].

One example from Fraunhofer IOF is the realization of a CPA using a Risley prism scanner [11]. As described in the paper, the realization of pointing for the technology used is affected by nonlinearities that must be taken into account in the design of the control loop. The tuning process of the actuators of the CPA itself is not discussed. Furthermore, it is not shown how to adjust the offloading dynamics from the FPA to the CPA in order to avoid instabilities in the individual control loops. It should also be noted that the maximum deflection achieved with the selected configuration is limited with 11 deg. According to the specified size, at least 6 units of the intended 12 unit CubeSat are occupied. However, the size and steering range are due to the intended use in an entangled quantum key distribution (QKD) mission. Therefore, it does not compete with the classical communication application discussed in this work.

In another work by TNO, the actuator principle of a switched reluctance motor is used, achieving a pointing jitter below 4 µrad root mean square (RMS) at a constant speed of 1 mrad s^{-1} [12]. It is also shown that the system consists of a gimbal-mounted deflecting mirror [13] and that its range accounts for ±180 deg in azimuth and ±20 deg in elevation. Further work discusses the effects of torque-induced ripple and how to overcome it [14]. In addition, a test bench was developed to validate the performance [15], but trajectory control aspects were not discussed.

The primary contribution of this work is the development of a decoupled trajectory controller with two distinct command sources and its verification with the actual CPA hardware. Section 2 details the design of the moving components of the CPA and the extrapolation procedure for ephemeris data. In that section, the offloading controller architecture is formulated. The subsequent Section 3 verifies the developed model and utilizes on-orbit data from an optical link to assess the performance of the offloading scheme. Additionally, the pointing performance of the CPA is analyzed for potential trajectory profiles that consider velocity and acceleration variations. Finally, Table 1 summarizes the SWaP and dynamic characteristics of state-of-the-art CPA designs for comparison.

2. Coarse pointing assembly design and dynamics

2.1. Coarse pointing assembly for CubeSat free-space optical communications

The strict SWaP requirements and constraints of the CPA, as depicted in Fig. 1, have led to a compact mechanical design with emphasis on commercial off-the-shelf (COTS) components and a novel ball-bearing preload system. The CPA consists of a dense flint glass prism glued to the elevation axis. The elevation axis is supported by a set of ball bearings and arranged perpendicular to the azimuth axis, as shown in Fig. 1. The azimuth axis is also supported by a respective set of ball bearings. Both bearing pairs are lubricated and axially face-to-face preloaded by a passive titanium spring system.

The elevation axis is driven by a 0.063 N m brushless direct current (BLDC) motor controlled by a COTS motor driver and features a 26 bit absolute encoder system with a ø 52 mm sensor scale ring. It covers a motion range of 80 deg. The azimuth axis has a 0.298 N m BLDC motor, a corresponding motor driver, and the same absolute 26 bit encoder with a ø 75 mm ring. Because the encoder, motor, and elevation servo drive are mounted on the azimuth axis, a flexible printed circuit (FPC) cable connects the azimuth axis to the satellite structure. The FPC cable is wrapped around the axis like a clock spring, limiting the range of motion to 356 deg. Both axes are locked during launch with a pin puller.

The use of a prism instead of a mirror allows nadir pointing for the CPA, meaning pointing in the local vertical direction aligned with gravity, while maintaining an envelope within a ø 64 mm times 36 mm cylinder with additional two-thirds of a unit occupied by the supporting structure

Optics EXPRESS

Table 1. CPA technologies designed for CubeSat systems

Model [Ref]	Size, mm	Weight, kg	Power, W	1σ, µrad	Range, deg	Slew, deg/s	C.A., mm	Tech.
Cube1G, DLR [18]	ø64×36 +2/3U[a]	1.5[a]	5-30[a]	2[h]	356/80 (Az/El)	360[b]	20	Gimbaled prism
CPA, TNO [12]	n/a	<5[a]	1-5[a]	4[f]	360/40 (Az/El)	n/a	70	Periscope
Cobalt, BlueCubed [19]	ø255×295	5.3	20-30	n/a	hyper-hemisphere	10	11	Gimbal
CubeEnik, IOF [11,20]	12U[c]	13.5[c]	11.4+[c]	n/a	22	0.05+[d]	80	Risley prism
MOSAIC, MIT [21]	500[e]	n/a	3+ [22]	n/a	360/<160 (Az/El)	n/a	$\frac{18}{1.4}$	Fisheye lens
Skylight, CACI [23]	1.5U	1.6	<35	n/a	100	n/a	n/a	n/a
LaserCube, Stellar [24,25]	3U	3.2	35-50	60[g]	20	n/a	40	Parallel manipu-lator

[a]SWAP values for CPA without LCT.
[b]Only limited by required trajectory tracking accuracy.
[c]Values for the double configuration LCT.
[d]Estimated from closed-loop behavior with (0.175 mrad · 57.32 deg rad^{-1})/0.2 s.
[e]Focus length for hemispherical steering.
[f]At 1^{-3} rev s^{-1}.
[g]At 1.6^{-4} rev s^{-1} (1 mrad s^{-1}/2π).
[h]At 1^{-3} rev s^{-1} and 0.1 rev s^{-2}.

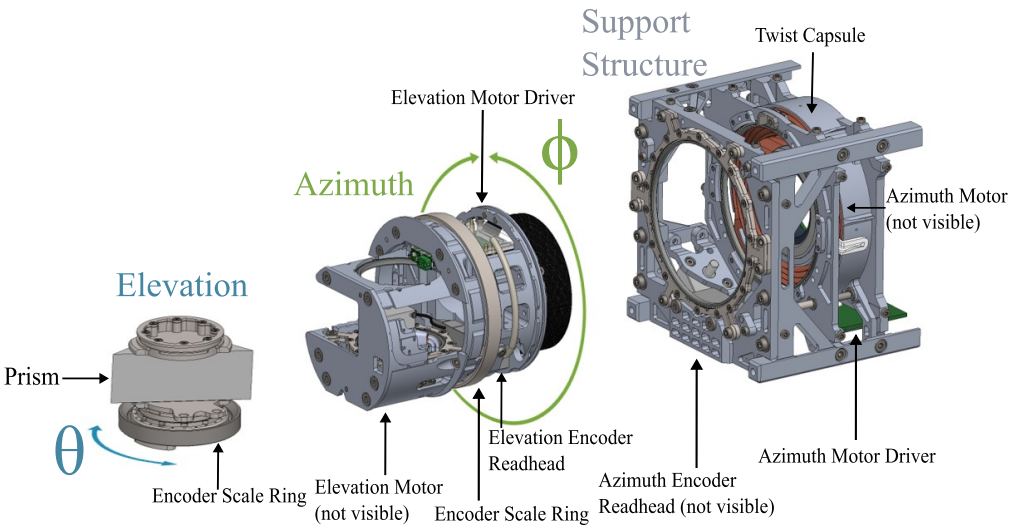

Fig. 1. Exploded view of the CPA with elevation axis, azimuth axis, and its supporting structure.

Optics EXPRESS

and a cable wrap. One unit (U) forms a cube with 100 mm edge length. In the latest design specification for CubeSats, required dimension specifications can be derived. According to the standard, it is possible to extend the maximal allowed box-shaped volume of a 6U CubeSat by a cylindrical extra volume called a tuna can. Placing a reflection prism inside the extra volume has the advantage that the free-space laser beam is not obstructed by parts of the satellite and a full hemispherical coverage is possible. The shape of the tuna can is one of the main design drivers and results in key differences in design compared to other CPAs in the literature.

2.2. Attitude and pointing determination

The CPA will be commanded by two different sources. The ephemeris data are used during the acquisition of the link. For this data source, pre-processing is necessary and will be explained in detail in this section. In Section 2.3 the s-curve profiler will be used to smooth this input. The other source of command is the offloading of the FPA within the system. Since the dynamics are coupled, a second-order linear time-invariant (LTI) system will be used to profile this input (see Sec. 2.3).

For open-loop pointing of the CPA during link acquisition, the setpoint angles ϕ_n, θ_n and their angular velocities $\dot{\phi}_n$, $\dot{\theta}_n$ at each time point t_n need to be provided to the profiler. The attitude determination and control system (ADCS) sends its timestamped position, velocity, and attitude at a frequency of 1 Hz. To provide the CPA trajectory control running at 20 Hz with more frequent updates, the data points from the satellite have to be extrapolated. The position and velocity are extrapolated using the Runge–Kutta 4 method, while the attitude uses linear extrapolation. The position of the target is required as well. In case of an optical ground station (OGS), its position in the International Celestial Reference System [16] is pre-calculated at 1 Hz for the link duration during link preparation and linearly interpolated to reduce the computational load. Based on the result, the setpoint angles ϕ_n and θ_n can be computed, as well as their velocities using ϕ_{n+1} and θ_{n+1}. After new satellite information has been received, the previously computed angles and velocities may not correspond to the actual values. This potential inconsistency has to be taken into account by the trajectory controller, as described in Section 2.3.

Another aspect is the time reference that has to be synchronized with the clock of the satellite, to ensure that no error is introduced in the ephemeris extrapolation and in the interpolation of the OGS position. A pulse-per-second signal of the satellite is used during the process to establish and maintain synchronization. This ensures that the extrapolated ephemeris data have an accuracy of ±1 deg or less, which is required to acquire the signal by the FPA in the envisaged scenario.

2.3. Trajectory controller design

The CPA will be used to perform pointing, as the initial phase, based on ephemeris data from the satellite. The coarse pointing will be supported by a scan pattern of the FPA to perform acquisition and to successfully establish a link. During the final tracking phase, the FPA will be used to perform closed-loop tracking. Meanwhile, the CPA's trajectory control will profile the coarse pointing based on estimated attitude data from the ADCS and, simultaneously, shape the commands for offloading the FPA.

In the initial phase, the CPA must follow the trajectory estimated from the satellite attitude and position data in combination with the desired target position, for example an OGS, as described in Section 2.2. For this pointing objective, an s-curve profiler is used to execute the ephemeris-based trajectory. This is based on the calculation of a fifth-order polynomial that takes into account the initial ϕ_0 and target ϕ_1 position and, analogously, the velocity ($\dot{\phi}_0$ and $\dot{\phi}_1$). In this example, the acceleration at the beginning and end of the profile is assumed to be zero. $\Delta\phi$ defines the position difference in the current time step interval T between ϕ_1 and ϕ_0. Note that, although jerk itself is not controlled in this profile, described by Eqs. (1)(a–d), the acceleration is kept

Optics EXPRESS

continuous and gradual:

$$P = \phi_0 + \dot{\phi}_0 t + \ddot{\phi}_0 t^2 + c_3 t^3 + c_4 t^4 + c_5 t^5, \tag{1a}$$

$$c_3 = \frac{4T^{-3}}{2}\left(5\Delta\phi - T\left(2\dot{\phi}_1 + 3\dot{\phi}_0\right)\right), \tag{1b}$$

$$c_4 = \frac{2T^{-4}}{2}\left(-15\Delta\phi + T\left(7\dot{\phi}_1 + 8\dot{\phi}_0\right)\right), \tag{1c}$$

$$c_5 = \frac{6T^{-5}}{2}\left(2\Delta\phi - T\left(\dot{\phi}_1 + \dot{\phi}_0\right)\right). \tag{1d}$$

A fifth-order polynomial is particularly suitable for s-curve profiling because it provides the minimum order necessary to achieve continuous position, velocity, acceleration, and jerk across the trajectory. This level of continuity is essential for smooth and physically realizable motion, especially in systems where abrupt changes in acceleration (i.e., jerk) can lead to undesirable dynamic effects. Lower-order polynomials, such as third-order, can ensure continuity in position and velocity, but they lack the flexibility to simultaneously constrain acceleration and jerk, often resulting in discontinuities that manifest as mechanical or control instabilities. The fifth-order formulation introduces six coefficients, which allow for the specification of initial and final conditions on position, velocity, and acceleration, while also inherently producing a continuous jerk profile. This makes it the lowest-order polynomial capable of producing a smooth s-curve transition with sufficient control over dynamic behavior. The coefficients c_3, c_4, and c_5 are then determined to satisfy end-point constraints on position, velocity, and acceleration, while ensuring a continuous acceleration profile.

In contrast to the trajectory control for the ephemeris data, the compensation of the offset angle of the FPA results in direct feedback via the optical path. It is therefore advisable to take these dynamics into account when designing the profiler. As an alternative to the conventional approach of using a PID controller for this task [17], a second-order LTI system is proposed (see Fig. 2).

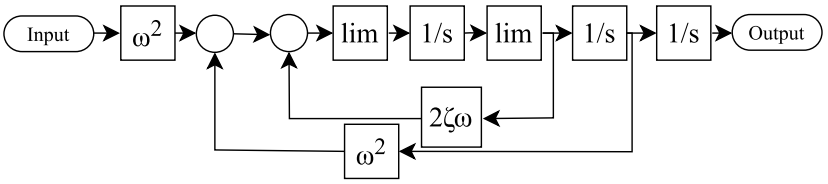

Fig. 2. Second-order LTI with additional integrating term to account for feedback coupling of the compensation in the FPA offloading angles and limiters (lim) to define maximum operating conditions. The input corresponds to the magnitude of angles for each axis of the FPA with respect to their central position, while the output is the angular command for the CPA to offload those angles.

Using the LTI system has the advantage that the system dynamics correspond to those of a mechanical system, and only the natural frequency ω has to be changed to tune the compensation behavior in an intuitive way. The damping should always follow an aperiodic behavior for the trajectory and is therefore set to $\zeta = 1$. However, if phase lag is important for the respective application, smaller damping values can be implemented. It is important to consider that this approach, whose lag is also a result of the two additional integration steps, requires additional computational resources. It is also possible to set limits for acceleration, velocity, and angle to account for mechanical system limits. The memory of the accumulated offset is realized by an additional integrator at the output. The proposed approach guarantees second-order behavior at

Optics EXPRESS

the output and decouples from the dynamics of the input source. In this case, the input source are the angles of the FPA, which are controlled via a dedicated control system. This means that the outputs to the CPA can be limited so that oscillation of the FPA cannot lead to a high-frequency change in commands. The simulation in Fig. 3 supports this, comparing the outputs of the controllers for a step function that changes its command value from one to zero after one second, as well as for sine signals with an amplitude of one and frequencies of 0.1 Hz, 1 Hz, and 10 Hz. The aperiodic behavior of the LTI system is especially visible in the first plot, while it has a lag of about 250 ms. In subsequent plots, the integrator follows the oscillating signal, while the LTI system settles on the mean value between the peaks of the oscillation, which is the favorable behavior.

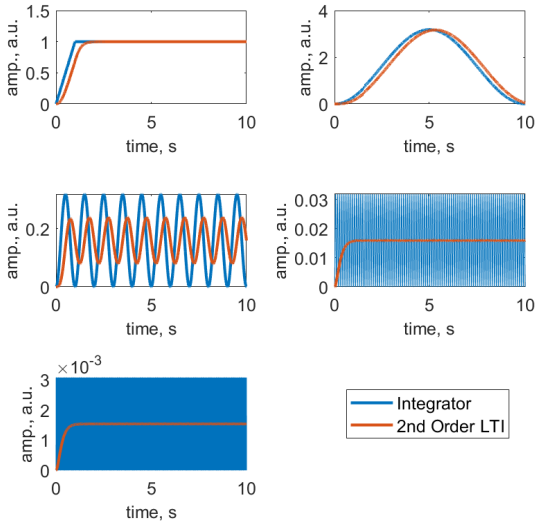

Fig. 3. Offloading control comparison between an integrator with gain one and the proposed LTI system with $\zeta = 1$, $\omega = 2\pi$ and internal limits of 0.1 rev s^{-1} and 1 rev s^{-2}.

2.4. *Gimbal low-level controller architecture*

The concept proposes that the CPA uses a servo controller as a low-level position control loop. This will be decoupled from the actual trajectory control so that error-tracking dynamics and trajectory dynamics can be set independently. The servo control consists of a classic cascaded system of P–PI–PI controllers (see Fig. 4). The position controller requires an angular velocity $(\dot{\phi}, \dot{\theta})$ from the velocity controller. The velocity controller then requires a torque τ from the current control loop. The current control loop uses feedback from the current i of the phases, which is transformed into direct and quadrature currents, to define the control voltage u. The velocity controller ensures zero steady-state error in velocity tracking, thereby indirectly eliminating steady-state position error when the remaining position error is significant enough. Including an additional integral term in the position loop is therefore redundant and may degrade system stability by increasing loop order and introducing phase lag.

It was decided to control the position because a pure velocity controller can generate an offset over the duration of a link if not compensated otherwise. The method of how to profile the movement from one extrapolated point to another is discussed in Section 2.3. The current low-level controller is set to achieve optimally damped behavior to achieve fast settling with $\zeta = 2^{-0.5}$. The velocity and position controller gains are set to ensure about 5 dB of gain margin. This margin is particularly important to account for changing conditions in the vacuum of space and temperature gradients due to uneven lighting conditions. For the position controller, the

Optics EXPRESS

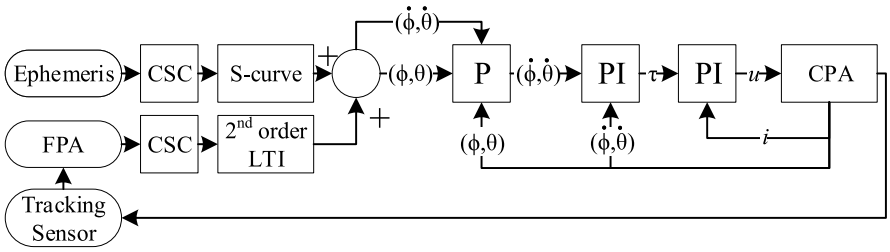

Fig. 4. The proposed trajectory controller combines an s-curve profiler for ephemeris data with a second-order LTI system for offloading—after a coordinate system conversion—and a low-level servo controller for CPA pointing.

resolution of the encoder is reduced from 26 bit to 24 bit to avoid numerical problems in the error calculation. This is not due to a signal processing effect but simply due to the minimal gain that can be achieved inside the microcontroller of the motor driver, which is a P gain of $1 \cdot 10^{-6}$ and therefore specific to the employed hardware.

3. Coarse pointing assembly hardware characterization

3.1. Plant identification

To validate the behavior of the hardware, a test setup consisting of the prototype of the CPA, the motor drivers, and the control software was built. In Fig. 5(d) the most relevant components are highlighted. The CPA is installed in the final frame. However, the enclosure shells are missing, which do provide additional stability to the structure and therefore increase the measured eigenfrequencies, as described later in this section.

A sinusoidal sweep is performed at 30% of the rated current of each motor to characterize the entire plant and compare it to the model. A frequency range from 15 Hz to 1 kHz is selected to get the relevant dynamics. The response shows the typical exponential decay of the amplitude as a result of the mass and inertia of the system, as well as deviations due to the surrounding structural resonances. The Bode plot for both azimuth and elevation (see Fig. 5) measurements is retrieved at several positions around the full actuation range.

It can be observed that the azimuth axis exhibits four distinct structural modes at 49 Hz, 69 Hz, 80 Hz, and 237 Hz. In contrast, the elevation axis shows only a single structural mode, which occurs at 258 Hz. This difference indicates a comparatively lower mass to stiffness ratio of the azimuth axis compared to the elevation axis. To place these results into context, a comparison is made with a fully integrated model of the system. Figure 5(c) presents the external resonance search performed on this complete model.

For the fully integrated LCT, the first eigenfrequencies are identified at 152 Hz for the elevation axis and 140 Hz for the azimuth axis. These modes represent the dominant dynamic behavior of the assembled structure. The second eigenfrequency of the azimuth axis is located at 349 Hz, followed by the first higher structural eigenfrequency at 528 Hz. Additional structural modes are observed at 654 Hz and 1092 Hz. Furthermore, several coupled eigenfrequencies involving both the azimuth and elevation axes are detected at 620 Hz, 996 Hz, and 1415 Hz.

Although a variety of structural and coupled modes are present across the measured frequency range, none of these resonances are considered critical for the control performance. This is because the targeted tracking bandwidth of the system is limited to 20 Hz, which lies well below the lowest identified eigenfrequencies. As a result, the influence of these higher-frequency structural modes on the error control behavior can be regarded as negligible.

Optics EXPRESS

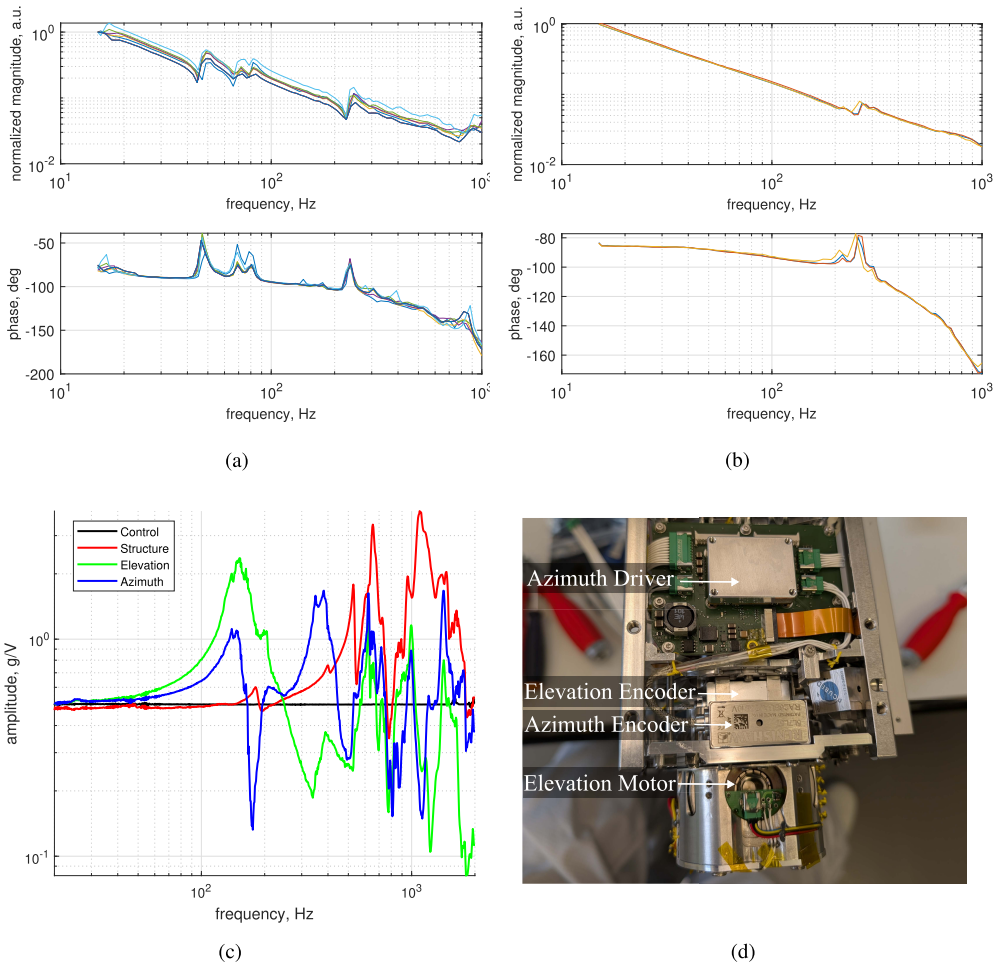

Fig. 5. Measured plants of (a) azimuth and (b) elevation axis, (c) lowest detected eigenfrequencies for all axes through resonance search with fully integrated model, and (d) CPA test setup for system identification and performance testing.

3.2. Offloading controller analysis

The retrieved transfer function of the CPA is coupled with a model of a relevant FPA. The example in Fig. 6 contains the FPA commands of an on-orbit direct-to-Earth (DTE) link [4]. This ensures that realistic input signals are used for validation. These are forwarded to the profiler at a frequency of 200 Hz, as in the actual application. The resulting offset angle of the FPA is analyzed. At a natural frequency ω of 100 Hz for the second-order LTI (see Fig. 2), the offloading becomes unstable. However, lower natural frequencies, starting from about 50 Hz, are feasible, such that the choice of the actual parameter then only depends on the required dynamics during offloading.

On one hand, the CPA should not try to compensate the FPA control noise, since this would imply stricter requirements on the mechanics and consume more energy. On the other hand, the FPA should not reach the limits of its control range. In the example above, all settings considered would be sufficient, with 1 Hz. It is also conceivable to implement a gain scheduler that adapts the choice of parameters to the dynamics of the link and counteracts more aggressively if the FPA gets too close to its deflection limit, in order to prevent the potential loss of the link.

Optics EXPRESS

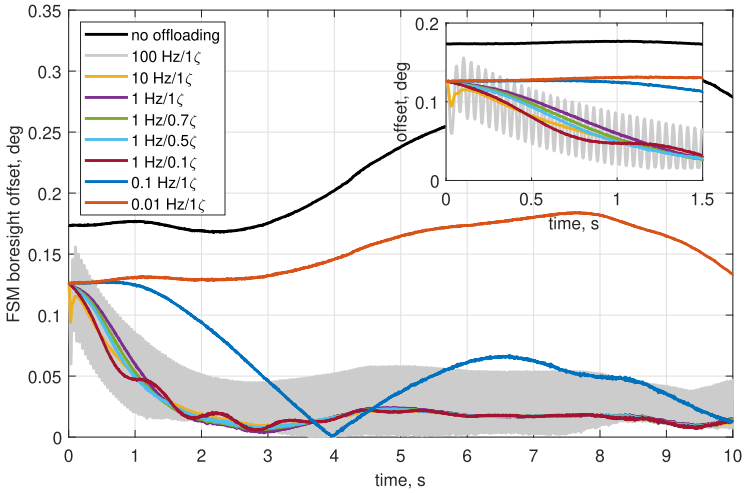

Fig. 6. FPA boresight offset from ideal orientation during offloading.

3.3. *System performance for dynamic trajectories*

As a second part, after simulating the second-order LTI trajectory controller, the s-curve profiler is analyzed using the test hardware. After performing a full-range test for both axes, it can be seen that an oscillatory behavior appears in the regulated current (see Fig. 7).

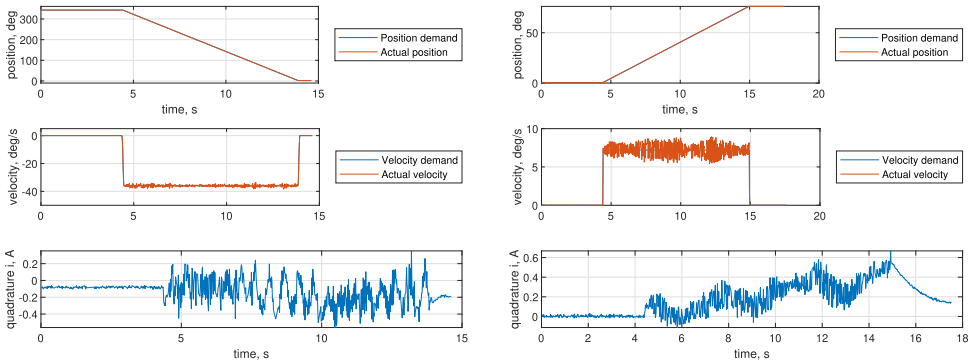

Fig. 7. Measured full-range example of (a) azimuth and (b) elevation axis with measured position, velocity, and quadrature current.

The number of periodic oscillations corresponds to the number of slots in the stator. This is an indication that the rotor has a slightly eccentric, non-circular run. This may be due to the manufacturing process or assembly. However, since it can be compensated for by the above controllers, it is negligible for this application.

Profiles for the trajectories can vary greatly, depending on the application scenario. This concerns DTE or inter-satellite link (ISL) as intra-plane or inter-plane configurations. Therefore, a number of possible acceleration and velocity profiles are combined and the determined RMS error is calculated from the acceleration to the deceleration phase. Figure 8 shows the dependence of the profiler settings on the accuracy requirements of the CPA, so that these can be taken into account in the design of the underlying FPA control loop. Note that these errors only account

Optics EXPRESS

for the open-loop pointing errors required for acquisition and do not represent the final optical closed-loop pointing error. One example of time-history data is embedded as a reference in the graph. The RMS error results in 2 µrad for this case. That result is the minimal position error for the measured velocity. However, a reference velocity for a standard low Earth orbit (LEO) DTE scenario at 500 km with nadir body pointing would require slew rates of approximately up to 0.9 deg s^{-1} which translates to 0.0025 rev s^{-1}. Assuming a linear increase between the measured velocities of 0.001 rev s^{-1} and 0.01 rev s^{-1} this results in a slew error standard deviation of about 9 µrad.

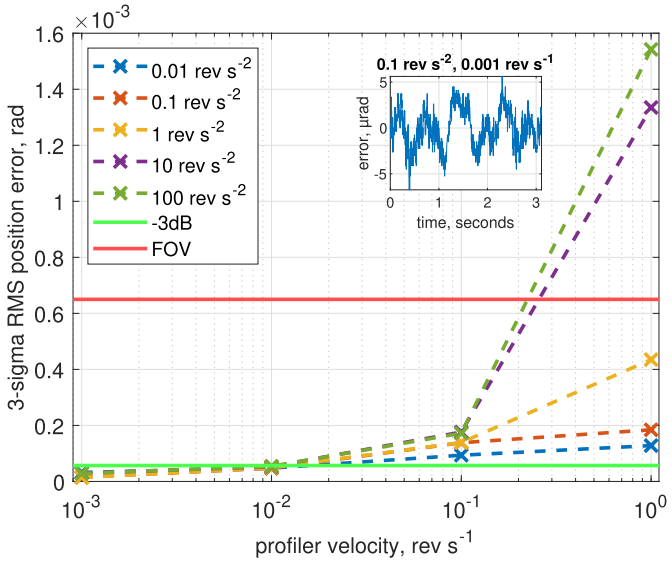

Fig. 8. 3σ RMS error of different s-curve profiler settings for the trajectory control and embedded time history of the position tracking error for the elevation axis with a profiler demanding 1 rev s^{-2} and 0.1 rev s^{-1}.

As demonstrated in the graphs, under the assumption of a specified FPA and field of view (FOV), along with a −3 dB pointing loss requirement as outlined in the actual mission, it can be observed that the control for both axes remains within the FOV limits at all times. This requires that the accelerations are within the range of 1 rev s^{-2} or below, and the velocities remain below 0.1 rev s^{-1}. Following these identified boundaries ensures that the risk of a tracking loss due to temporary errors in acceleration and velocity following, and therefore pointing, is minimized. For limited accelerations, FOV tracking requirements of 650 µrad are maintained for the maximum tested velocity of 1 rev s^{-1}. Furthermore, both axes are close to or below the −3 dB divergence limit of 56.75 µrad up to a maximum acceleration of 100 rev s^{-2} and a maximum velocity of 0.01 rev s^{-1}. Consequently, within the mentioned limits, relying exclusively on the precision of the CPA is sufficient for acquiring the desired link.

A selection of ongoing developments for CPAs is listed in Table 1, which are usually designed together with an LCT. This approach is commonly pursued, since the design of the CPA strongly depends on the interface to the LCT. Therefore, they are listed with the corresponding LCT model.

In terms of physical size and mass, solutions for classical communication on CubeSats such as Cube1G and Skylight exhibit the most compact form factors, with the lowest volume of 1.5U for Skylight. With 2U plus ø 64 mm times 36 mm, the complete Cube1G LCT is the second most compact design with a clear aperture of 20 mm. Skylight also achieves the lowest mass with 1.6 kg for the LCT assembly. It is difficult to assess the power consumption because it varies

Optics EXPRESS

greatly between high dynamic pointing maneuvers and steady slew rates. Additionally, reference sources usually provide the power budget for the entire LCT.

Pointing accuracy varies substantially across the surveyed systems. High-precision solutions such as Cube1G and the TNO CPA solution report 1σ pointing errors of only a few microradians, whereas LaserCube exhibits comparatively less accurate coarse pointing (60 µrad).

Regarding angular coverage, gimbaled and periscope-based architectures generally provide near or full azimuthal coverage with elevation ranges between 40 deg and 80 deg forming a hyper-hemisphere. Risley-prism-based systems such as CubeEnik exhibit more restricted angular ranges but benefit from mechanically compact CPA designs and large clear apertures. Fisheye-based concepts, exemplified by MOSAIC, achieve extremely wide FOV with minimal motion, trading optical complexity and calibration challenges for mechanical simplicity.

Dynamic performance, expressed in terms of slew rate, also shows considerable variation. Compact gimbaled systems such as Cube1G support very high slew rates of up to 360 deg s^{-1}, making them well suited for agile tracking scenarios. By contrast, Risley prism systems generally exhibit much lower slew capabilities, since they need to account for nonlinearities in the optical system design.

Overall, the table highlights the inherent trade-offs between compactness, pointing accuracy, angular coverage, and dynamic performance. No single architecture can optimize all metrics simultaneously. Instead, each design is a compromise tailored to specific mission requirements. This comparison highlights the importance of carefully selecting terminal architecture based on targeted platform constraints and operational scenarios.

4. Conclusion

The gimbaled-prism-based CPA enhances CubeSat optical communications by enabling near-hemispherical pointing independent of satellite body orientation. Its hierarchical control approach, combining a servo loop with separate trajectory controllers, ensures precise pointing while offloading errors from the FPA. The ephemeris trajectory controller enables smooth CPA motion, while the second-order LTI controller dynamically compensates for residual errors without excessive jitter or actuator loading. Based on the FOV requirement, the CPA is able to keep the tracking error within the limits up to the maximum tested velocity of 1 rev s^{-1} for limited accelerations. However, 2 µrad is achievable for slower profiles and 9 µrad for pointing maneuvers that are within DTE link dynamics. Overall, the proposed control scheme balances long-term trajectory execution and offloading with real-time error correction, improving robustness and operational independence for CubeSat optical links.

Funding. Bundesministerium der Verteidigung; European Union (NextGenerationEU).

Acknowledgment. This research work is funded by dtec.bw – Digitalization and Technology Research Center of the Bundeswehr – and has been supported partially by the German Federal Ministry of Defense through the technological research and development assignment “Responsive Space Capabilities”. Dtec.bw is funded by the European Union – NextGenerationEU.

The authors would like to thank Manfred Schedl and Bernhard Thaler for their invaluable support during the commissioning of the coarse pointing assembly.

Disclosures. The authors declare no conflicts of interest.

Data availability. Data underlying the results presented in this paper are not publicly available at this time but may be obtained from the authors upon reasonable request.

References

1. T. S. Rose, D. W. Rowen, S. D. LaLumondiere, *et al.*, “Optical communications downlink from a low-earth orbiting 1.5u cubesat,” Opt. Express **27**(17), 24382–24392 (2019).
2. W. Kammerer, P. Grenfell, J. Harburg, *et al.*, “Click-a: Optical communication experiments from a cubesat downlink terminal,” *Small Satellite Conference* (2023).

Optics EXPRESS

3. K. M. Riesing, C. M. Schieler, J. S. Chang, *et al.*, "On-orbit results of pointing, acquisition, and tracking for the tbird cubesat mission," in *Free-Space Laser Communications XXXV*, H. Hemmati and B. S. Robinson, eds. (SPIE, 2023), Proceedings of SPIE, p. 4.
4. R. Rüddenklau, F. Rein, C. Roubal, *et al.*, "In-orbit demonstration of acquisition and tracking on osiris4cubesat," Opt. Express **32**(23), 41188–41200 (2024).
5. J. du Plooy, J. Hejderup, S. Engelen, *et al.*, *Assessing the Results of a Space-To-Ground Data Transfer Link of a 1U Laser Communication Terminal for SmallSats* (Small Satellite Conference, 2024).
6. Y. Kim, P. Kim, H.-G. Ryu, *et al.*, "Gps-based relative navigation for laser crosslink alignment in the vision cubesat mission," Aerospace **12**(10), 928 (2025).
7. P. Martín Pimentel, B. Rödiger, C. Schmidt, *et al.*, "Cube laser communication terminal (cubelct) state of the art," Acta Astronaut. **211**, 326–332 (2023).
8. E. D. Miller, M. DeSpenza, I. Gavrilyuk, *et al.*, "A prototype coarse pointing mechanism for laser communication," in *Free-Space Laser Communication and Atmospheric Propagation XXIX*, H. Hemmati and D. M. Boroson, eds. (SPIE, 2017), SPIE Proceedings, p. 100960S.
9. R. Barho and M. Schmid, "Coarse Pointing and Fine Pointing mechanism (CPA and FPA) for an optical communication link," in *10th European Space Mechanisms and Tribology Symposium*, vol. 524 of *ESA Special Publication* R. A. Harris, ed. (2003), pp. 89–96.
10. T. T. Nielsen, "Pointing, acquisition, and tracking system for the free-space laser communication system silex," in *Free-Space Laser Communication Technologies VII*, G. S. Mecherle, ed. (SPIE, 1995), SPIE Proceedings, p. 194.
11. P. Krause, D. Heinig, M. Goy, *et al.*, "A compact pointing assembly for a cubesat to ground station free-space optical communication based on a risley prism scanner coarse and a tip/tilt mirror fine pointing," in *Environmental Effects on Light Propagation and Adaptive Systems VI*, K. Stein and S. Gladysz, eds. (SPIE, 2023), p. 21.
12. L. Kramer, J. Peters, R. Voorhoeve, *et al.*, "Novel motorization axis for a coarse pointing assembly in optical communication systems," IFAC-PapersOnLine **53**(2), 8426–8431 (2020).
13. R. Saathof, S. Kuiper, W. Crowcombe, *et al.*, "Opto-mechatronics system development for future intersatellite laser communications," in *Free-Space Laser Communications XXXI*, H. Hemmati and D. M. Boroson, eds. (SPIE, 2019), p. 47.
14. N. Mooren, M. van Meer, G. Witvoet, *et al.*, "Compensating torque ripples in a coarse pointing mechanism for free-space optical communication: A gaussian process repetitive control approach," Mechatronics **97**, 103107 (2024).
15. M. Dresscher, J. D. Human, G. Witvoet, *et al.*, "Key challenges and results in the design of cubesat laser terminals, optical heads and coarse pointing assemblies," in *2019 IEEE International Conference on Space Optical Systems and Applications (ICSOS)* (IEEE, 2019), pp. 1–6.
16. IERS (International Earth Rotation and Reference System Service), "Technical Note No. 23: Definition and Realization of the International Celestial Reference System by VLBI Astrometry of Extragalactic Objects," (1997).
17. H. Hemmati, *Near-Earth laser communications*, Optical science and engineering (CRC Press, 2021), 2nd ed.
18. L. R. Rodeck, F. Rein, R. Rüddenklau, *et al.*, "Cube1g: a full-hemispherical, high-speed optical communication terminal for cubesats," *76th International Astronautical Congress* (IAC 2025).
19. BlueCubed, "Cobalt + gimbal,".
20. E. Beckert, D. Heinig, F. Steinlechner, *et al.*, "Ultra-compact payload for a leo-orbit based entanglement qkd mission using cubesats," in *Quantum Computing, Communication, and Simulation V*, P. R. Hemmer and A. L. Migdall, eds. (SPIE, 2025), Proceedings of SPIE, p. 30.
21. S. Kacker and K. Cahoy, "Liquid lenses for aerospace beam steering and communications: Mosaic," Opt. Express **33**(1), 1296–1313 (2025).
22. Optotune, "El-16-40-tc lens," (accessed 2026-02-10).
23. CACI, "Skylight™optical communication," (accessed 2026-02-10).
24. Stellar Project, "Lasercube," (accessed 2026-02-10).
25. F. Sansone, A. Francesconi, R. Corvaja, *et al.*, "Lasercube optical communication terminal for nano and micro satellites," Acta Astronaut. **173**, 310–319 (2020).